

CDF-Glove: A Cable-Driven Force Feedback Glove for Dexterous Teleoperation

Anonymous Author(s)

Abstract—High-quality teleoperated demonstrations are a primary bottleneck for imitation learning (IL) in dexterous manipulation. However, haptic feedback allows operators to perceive real-time contact haptic during dexterous teleoperation and adjust finger poses, which can improve demonstration quality. Existing dexterous teleoperation platforms typically omit haptic feedback and exhibit unfavorable size and cost profiles. We introduce CDF-Glove, a lightweight and low-cost cable-driven force-feedback glove. Real-time state is available for 20 finger degrees of freedom (DoF), of which 16 are directly sensed and 4 are passively coupled (inferred from kinematic constraints). We develop a kinematic model and control stack for the glove and validate motion control on multiple robotic hands with diverse kinematics and DoF. CDF-Glove costs approximately \$230, achieves distal-joint repeatability of 0.4° , and delivers about 200 ms force-feedback latency, yielding a 4x improvement in task success rate relative to no-feedback teleoperation. We collect two bimanual teleoperation datasets and train and evaluate an IL baseline using Diffusion Policy. Compared to kinesthetic teaching, policies trained on our teleoperated demonstrations increase the average success rate by 55% and reduce the mean completion time by 15.19 seconds (a 47.2% relative reduction). Code and designs will be released as open source at <https://cdfglove.github.io/>.

I. INTRODUCTION

Imitation Learning (IL) [1] has emerged as a powerful paradigm for solving complex dexterous manipulation tasks, yet its success is critically dependent on the availability of high-quality expert demonstration data. Data gloves [2] present an intuitive method for capturing human hand kinematics for this purpose. However, the performance of the resulting IL policy hinges critically on the quality and dimensionality of the captured data. This motivates the development of a teleoperation system capable of recording high-dimensional hand joint data with high precision. Furthermore, haptic feedback [3] is critical, as it enables the operator to perceive interaction haptic during grasping and manipulation. This closed-loop control allows the operator to make nuanced adjustments to their manipulation strategies, thereby significantly enhancing the quality and effectiveness of the collected demonstration data. Despite its importance, existing high-DoF haptic gloves [4], [5] present a challenging trade-off: they are often either prohibitively expensive, limited in sensing dimensionality and actuated DoF, or lack haptic feedback entirely. Moreover, many existing systems neglect crucial aspects of usability, such as wearability, comfort, and inherent safety, which limits their practical application for long-duration data collection. To address these limitations, this work introduces the **CDF-Glove**: a lightweight, low-cost, and high-DoF haptic glove. Our design leverages a cable-driven mechanism, which offers inherent



Fig. 1: The CDF-Glove and the whole machine teleoperation system. The CDF-Glove is worn on the user's hand to collect hand joint data and provide haptic feedback.

safety, rapid response times, and a simple structure conducive to easy replication. Subsequently, the kinematics of the cable-driven finger measurement system and the tracking of force-feedback cables are modeled and analyzed. Finally, a series of experiments are conducted to verify the performance of the CDF-Glove. Bimanual data collection is performed using the CDF-Glove. The collected data are utilized for IL training to verify both the high quality of the data and the effectiveness of the Diffusion Policy [6].

This work offers the following contributions:

- The design and implementation of the CDF-Glove, a novel, lightweight, high-DoF, and inherently safe haptic glove with an integrated haptic feedback system, developed at a total cost of only \$230. The device achieves a distal joint positioning repeatability of 0.4° and a haptic feedback response time of 200 ms.
- A comprehensive kinematic model that maps cable displacement to finger joint angles, alongside a tracking model for the force-feedback transmission system.
- An extensive experimental validation demonstrating that IL policies trained with data collected by the CDF-Glove significantly outperform those from kinesthetic teaching (KT). Specifically, our method improves the task success rate by 55% percentage points and reduces the average completion time by 15.19 seconds (a 47.2% relative reduction).

II. RELATED WORK

A. General Demonstration Teleoperation

In the field of teleoperation, various data collection methods have been explored.

The VR-based approach [7]–[10] is simple and easy to deploy, making it suitable for rapid development and testing. However, it suffers from poor dynamic performance,

especially during fast movements or complex tasks, leading to latency and data loss. Additionally, it lacks precision in mapping the hand posture, which is crucial for high-precision dexterous operations.

The motion capture approach using cameras [11]–[13] provides intuitive operation and can capture overall movements well. However, it falls short in accurately mapping hand movements, especially the fine details of finger actions. Its dynamic performance is average, and the high cost of motion capture gloves limits its practical application.

The methods of them are costly. Although these methods have strong algorithm generalization capabilities, they still suffer from latency issues during fast movements, which can affect the smoothness and accuracy of operations. Moreover, these methods are often not precise enough for fine movements and lack haptic feedback, making it difficult for users to accurately judge and adjust their strategies when performing complex tasks.

B. Wearable Devices for Teleoperation

Many studies have also utilized wearable devices for data collection in teleoperation.

The combination of exoskeleton arms with grippers or exoskeleton hands [14]–[16] offers lower hardware costs but results in a more complex system that is difficult to maintain. These systems are often bulky, restricting the user's range of motion and reducing operational flexibility. Moreover, their interaction performance, particularly in haptic feedback, is not satisfactory, leading to an unnatural user experience. On the other hand, exoskeletons with linkages [17]–[20] are mostly bulky and heavy, with complex wearing procedures that can negatively impact user experience, which resulting in low-quality data collection. Additionally, the kinematics calculations for these exoskeletons are complicated.

Furthermore, the cost of Zhang et al.'s [4] exoskeleton is still not low enough, and its significant weight can affect the user's experience and, consequently, the precision of the collected data. Meanwhile, many cable-driven exoskeletons [21], [22] lack accurate position sensing or have complex control mechanisms, resulting in limited data collection and low DoF.

To address these limitations, we propose a data collection method for dexterous teleoperation using CDF-Glove equipped with trackers. This glove is lightweight, low-cost, easy to maintain and has a high DoF. It provides high-precision data collection for hand joints with low latency, ensuring good dynamic performance. The end-effector mapping is concise and accurate, supporting high-precision teleoperation tasks. This solution offers both cost-effectiveness and improved performance, making it a more viable option for teleoperation applications.

III. MECHANICAL DESIGN

A. Design Requirements and Approach

The CDF-Glove is a wearable device designed to accurately capture human hand motion. While maximizing the acquisition of joint angle data and maintaining high fidelity,

the device aims to minimize weight and volume, resulting in a more compact and lightweight structure to ensure user comfort. To improve data acquisition reliability, the device incorporates a closed-loop system that provides the user with real-time feedback on capture status and quality.

To meet these design requirements, the CDF-Glove employs a cable-driven mechanism to measure joint angles. This design obviates bulky finger-mounted linkages by consolidating components on the back of the hand. Moreover, the low latency inherent to cable transmission is critical for achieving real-time data acquisition. Integrating cable-driven mechanisms into the haptic feedback system further enhances user safety. When abnormal data are detected or excessive external force is applied, the cable can automatically relax to prevent injury to the user's hand.

Given the characteristics of the CDF-Glove, it is divided into a measurement system in Sec. III-B and a force feedback system in Sec. III-C.

B. Measurement System

Many studies [23] have modeled the kinematics of the human hand. As shown in Fig. 2(b), the hand mainly consists of hinge joints and ball-and-socket joints. Each of the index, middle, ring, and pinky fingers features two 1-DoF hinge joints—the distal interphalangeal (DIP) and proximal interphalangeal (PIP)—that perform bend. Their metacarpophalangeal (MCP) joint is a 2-DoF joint, enabling both bend and split. The thumb differs slightly: both the IP and MCP joints permit only bending, whereas the trapeziometacarpal (TM) joint is a saddle joint that allows both bending and split motions. Additionally, the wrist provides two DoF.

Based on these anatomical features and joint arrangements, we designed an exoskeleton glove system, CDF-Glove, as illustrated in Fig. 2(a). The wrist is tracked using the HTC VIVE Tracker 3.0, which is shown semi-transparently in the figure. After rigidly attaching the hand cover shown in Fig. 3 to the glove, the assembly is worn on the user's hand. It integrates 16 active measured DoF and 4 passive DoF (PIP). As depicted in Fig. 2(c), the kinematic model of each hand joint is mapped onto the CDF-Glove. Joint data are acquired using RDC506018A encoders. For the index, middle, ring, and pinky fingers, the split motion of the MCP joint is directly measured by encoders, as shown in Fig. 3. For the thumb, both DoF of the TM joint are also measured by encoders.

The structure of each finger, depicted in Fig. 4, primarily consists of non-standard components 3D-printed from PLA for a lightweight and low-cost design. Each phalanx is equipped with a dedicated sleeve, which attaches securely to the finger via a snap-fit mechanism to prevent slippage and rotation. Adjacent phalangeal sleeves are connected by the connecting spring (spring 1), which not only links the sleeves but also enables faster force feedback reset. The wire diameter of spring 1 is small, resulting in low stiffness that can be neglected during operation, thus minimizing interference with natural hand movements.

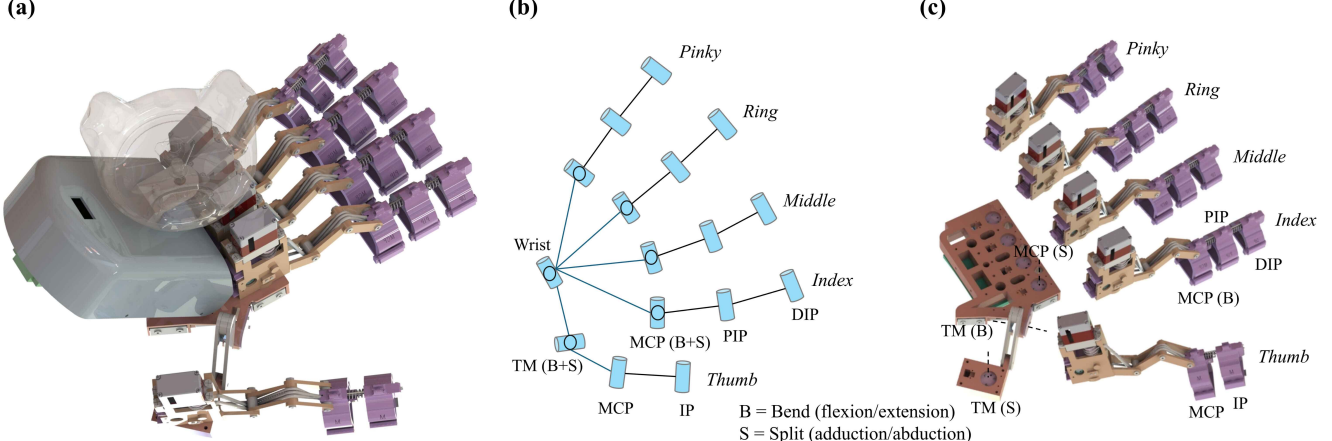


Fig. 2: Overview of the CDF-Glove system. (a) Overall structural diagram of the CDF-Glove system. (b) Kinematic structure of the human hand system. (c) Overall kinematic layout of the CDF-Glove system.

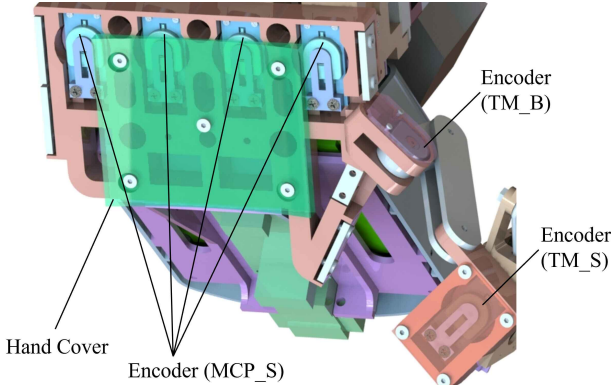


Fig. 3: Arrangement of encoders at the base of the fingers.

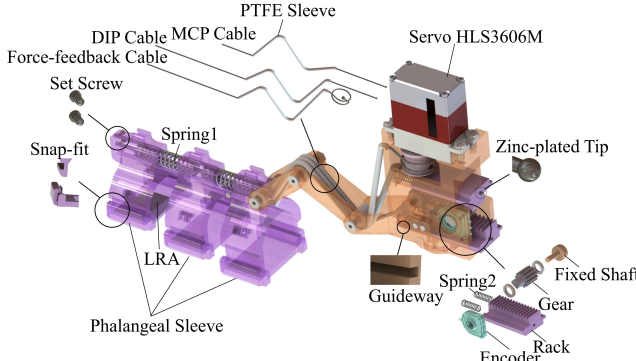


Fig. 4: Exploded view of the single-finger structure.

To measure the angles of the DIP and MCP joints, two steel cables with zinc-plated tips and a diameter of 1 mm are routed through the DIP and MCP joints, respectively. These cables are guided by polytetrafluoroethylene (PTFE) sleeves to effectively reduce friction [24]. One end of each cable passes through the reset spring (spring 2) and is secured to a rack by the zinc-plated tip. The rack slides along a guideway, driving a 12-tooth gear to rotate, thereby changing the encoder readings. The moderate stiffness of spring 2 avoids significant interference with hand operation, ensures

encoder reset, and effectively prevents cable slack during tensioning, thereby maintaining measurement accuracy. The opposite end of the steel cable is fixed to the phalangeal sleeve using a set screw. After an initial pre-tensioning, the system does not require further adjustment during an operational session. Specifically, the MCP and DIP cable are fixed to their phalangeal sleeves, enabling independent measurement of DIP and MCP joint angles. The calculation method for the PIP angle will be described in Sec. IV-A.

C. Force Feedback System

Our device integrates a dual-mode haptic feedback system, combining vibrotactile feedback from Linear Resonant Actuators (LRAs) with kinesthetic force feedback from a cable-driven mechanism, as illustrated in Fig. 4, which together constitute the haptic and cable-driven force feedback system. The system employs two distinct types of actuators: LRAs provide vibrotactile feedback directly to the user's fingertip, while servos drive a cable-transmission system to generate kinesthetic force feedback. When the dexterous hand equipped with force sensors transmits signals to the main control board, the force feedback mechanism is activated, as summarized in Table. I.

The LRA is embedded beneath the DIP phalangeal sleeve, allowing direct contact with the user's fingertip to deliver high-frequency haptic feedback. Depending on the measured force, the LRA automatically adjusts the frequency of its driving signal, producing different waveforms to achieve various haptic feedback effects. As shown in Table. I, the LRA driving signals are divided into two ranges: 0.1~0.5 N (Waveform 1) and 0.5~1 N (Waveform 2).

The FEETECH HLS3606M servo provides a stall torque of 6 kg·cm, which is sufficient to meet the requirements. One end of the force-feedback cable is fixed to the DIP phalangeal sleeve with a set screw, while the other end is connected to the output flange, passing through the PTFE sleeve. The servo drives the output flange, tightening the cable and generating force feedback. The tension in the cable can be adjusted by the servo's rotation, enabling different

TABLE I: Haptic Feedback Strategy of CDF-Glove

Force Sensor Readings (N)	Vibration Feedback	Force Feedback
< 0.1	—	—
0.1~0.5	✓(Waveform 1)	—
0.5~1	✓(Waveform 2)	—
> 1	—	✓

levels of force feedback. When the finger bends, the cable elongates, and the amount of elongation is calculated using the formula described in Sec. IV-B.

IV. SYSTEM MODELING

A. Kinematic Model of Finger Joint

To retarget motion to a dexterous robotic hand, we first establish a kinematic model of the CDF-Glove. This model computes the user’s finger joint angles from the device’s encoder readings. As shown in Fig. 5(a), only the angles of the MCP and DIP joints are directly measured, while the PIP joint angle is correlated with the DIP joint angle [25], as reflected in (2). Therefore, the PIP joint angle can be computed from the DIP joint angle. The kinematic model can thus be formulated as follows:

$$\begin{aligned} \theta_1 &= \frac{\Delta P_1}{r_1}, \\ \Delta P_1 &= r_g \cdot \theta_{e_m}, \\ \Delta L'_1 &= \theta_1 \cdot r'_1 \end{aligned} \quad (1)$$

$$\begin{aligned} \theta_2 &= \frac{\theta_3 + 0.230}{0.989}, \\ \Delta L'_2 &= \theta_2 \cdot r'_2 \end{aligned} \quad (2)$$

$$\begin{aligned} \theta_3 &= \frac{\Delta L'_3}{r'_3}, \\ \Delta P_3 &= r_g \cdot \theta_{e_d}, \\ \Delta P_3 &= \Delta L'_1 + \Delta L'_2 + \Delta L'_3 \end{aligned} \quad (3)$$

where θ_1 , θ_2 , and θ_3 represent the angles of the MCP, PIP, and DIP joints, respectively. ΔP_1 and ΔP_3 denote the cable displacements at the MCP and DIP joints, respectively. r'_1 , r'_2 , and r'_3 are the effective radii of the DIP measurement cable at the MCP, PIP, and DIP joints, with values of 23.25 mm, 19.31 mm, and 17.42 mm, respectively. r_1 is the effective radius of the MCP measurement cable at the MCP joint, with a value of 16.25 mm. r_g denotes the radius of the gear connected to the encoder. θ_{e_m} and θ_{e_d} are the angles measured by the encoders at the MCP and DIP joints, respectively. $\Delta L'_1$, $\Delta L'_2$, and $\Delta L'_3$ represent the elongations of the DIP measurement cable at the MCP, PIP, and DIP joints, respectively, when the finger is fully flexed. The constants 0.230 and 0.989 in (2) are obtained experimentally [25]. By solving these kinematic equations, we obtain the user’s finger joint angles, which are subsequently mapped to the dexterous hand for real-time control.

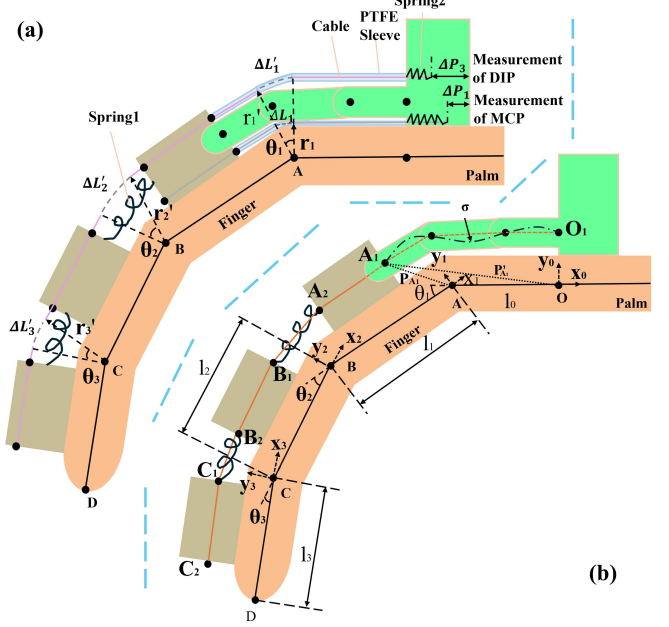


Fig. 5: Kinematic model for a single finger joint in the flexed position. (a) Schematic of joint angle calculation for an individual finger. (b) Force-feedback cable following calculation based on fingertip position localization.

B. Force-feedback Cable Following Calculation

In our force feedback system, the servo must actively manage the force-feedback cable to follow the user’s natural finger movements. For instance, when the user’s finger flexes, the cable path along the dorsal side elongates, requiring the servo to pay out the cable to maintain a constant tension. Conversely, when the finger extends, the cable path shortens, and the servo must retract the cable to take up slack. Accurately calculating this required cable displacement is essential for transparent operation. To enable this motion following, the system must continuously compute the target displacement of the force-feedback cable. This displacement is calculated directly from the finger’s posture—specifically, the joint angles derived in the previous section. The geometric model for this calculation, illustrated in Fig. 5(b), is based on the coordinate transformations detailed below:

$$\theta_s = \frac{L_a}{r_s} \quad (4)$$

$$\begin{aligned} L_a &= |P'_{A_1} - P'_{O_1}| + |P'_{A_2} - P'_{A_1}| + |P'_{B_1} - P'_{A_2}| \\ &\quad + |P'_{B_2} - P'_{B_1}| + |P'_{C_1} - P'_{B_2}| + |P'_{C_2} - P'_{C_1}| + \sigma \end{aligned} \quad (5)$$

$$\begin{aligned} P'_{A_1} &= T_{01} P_{A_1}, \\ P'_{A_2} &= T_{01} P_{A_2}, \\ P'_{B_1} &= T_{01} T_{12} P_{B_1}, \\ P'_{B_2} &= T_{01} T_{12} P_{B_2}, \\ P'_{C_1} &= T_{01} T_{12} T_{23} P_{C_1}, \\ P'_{C_2} &= T_{01} T_{12} T_{23} P_{C_2} \end{aligned} \quad (6)$$

$$T_{n-1,n} = \begin{bmatrix} \cos \theta_n & -\sin \theta_n & 0 & -l_{n-1} \\ \sin \theta_n & \cos \theta_n & 0 & 0 \\ 0 & 0 & 1 & 0 \\ 0 & 0 & 0 & 1 \end{bmatrix} \quad (7)$$

where θ_s denotes the rotation angle of the servo, and r_s represents the radius of the output flange. L_a represents the length of the force-feedback cable with respect to the base coordinate origin O . $P_{A_1}, P_{A_2}, P_{B_1}, P_{B_2}, P_{C_1}$, and P_{C_2} denote the vectors of the corresponding points with respect to the local coordinate systems at points A, B, and C, respectively. l_0, l_1, l_2, l_3 are the lengths of the segments between the base coordinate origin O , the points A, B, C, and D, respectively. Their lengths are 35.71 mm, 44.33 mm, 24.21 mm, and 23.51 mm, respectively. $P'_{A_1}, P'_{A_2}, P'_{B_1}, P'_{B_2}, P'_{C_1}$, and P'_{C_2} are the vectors of the corresponding points with respect to O . σ is a cable slack variable, typically set to 2 mm. $T_{n-1,n}$ is the transformation matrix from coordinate frame $n - 1$ to frame n . The angle θ_n and length l_{n-1} are defined according to the kinematic model of the finger joints, where θ_n is obtained from Sec. IV-A. Through the transformations in (6), the local coordinates can be converted to global coordinates. Once the value of L_a is obtained, the θ_s can be calculated using (4), thereby enabling precise determination of the target force-feedback cable displacement.

V. EXPERIMENTS

In this section, experiments are conducted to validate the performance of the CDF-Glove in Sec. V-A, Sec. V-A.1, V-A.2, and V-A.3 present the basic control demonstration, haptic feedback performance, and repeated positioning performance, respectively. Then we validate the effectiveness of the kinematic model and force-feedback cable following calculation proposed in Sec. IV (see Sec. V-B). Data are collected through bimanual teleoperation tasks (see Sec. V-C), and the validity of the data is evaluated using Diffusion Policy (see Sec. V-D). The overall parameters of the CDF-Glove are presented in Table. II, and the cost is summarized in Table. III.

A series of experiments are conducted on a bimanual humanoid robot. As shown in Fig. 6, the CDF-Glove is used to teleoperate the RY-H1 dexterous hand from RUIYAN, which features 15 actively actuated DoF. The maximum data acquisition frequency of the CDF-Glove is approximately 100 Hz. Wrist tracking is accomplished using the HTC Vive Tracker 3.0 and the HTC Vive Lighthouse 2.0, with 6D pose estimation provided by SteamVR.

TABLE II: CDF-Glove Overall Performance Parameters

Items	Parameters
Weight (including servos)	0.49 kg
Force feedback latency to hand	200 ms
Measurable DoF	16
Coupled computation DoF	5
Finger width	25 mm
Communication protocol	RS485 & Modbus @ 0.5Mbps/s
Maximum Power	50 Watt @ 5 Volt

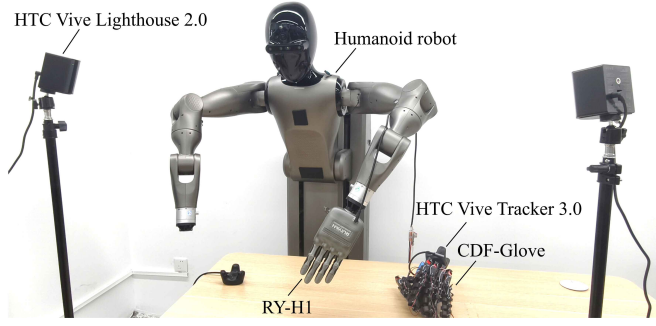


Fig. 6: Overview of the complete experimental test system.

TABLE III: Cost of CDF-Glove and Others'

Type	Item	Num	Price
Electronic components	Control board	1	\$90.2
	Servos HLS3606M	5	\$107.1
	LRAs	5	\$7.14
	Encoders	16	\$4.13
Non-standard parts	3D printed parts		\$14.28
	Other materials		\$3.03
Other components	Cable	15	\$8.65
	Screws		\$0.35
	Gaskets		\$0.09
	PTFE sleeves		\$0.11
	Springs		\$4.08
Total cost			\$230.51
DOGlove [4]			\$600
GEX Series [26]			\$600

A. CDF-Glove Performance Validation

1) *CDF-Glove Basic Control Demonstration:* To verify the effectiveness of teleoperated motion mapping with the CDF-Glove, a basic control demonstration experiment is conducted. In this experiment, the user wears the CDF-Glove and controls the RY-H1 by performing corresponding finger joint movements. Fig. 7 illustrates the split motion of the MCP joint, the bend motion of the MCP joint, and the bend motion of the DIP joint, respectively. The results demonstrate successful teleoperation. The RY-H1 hand visibly mirrored the user's finger movements with no perceivable latency. The system proved capable of mapping a variety of gestures, from individual joint motions to complex grasping postures.

2) *CDF-Glove Force Feedback Performance:* To validate the haptic feedback performance of the CDF-Glove, as described in Sec. III-C and Sec. IV-B, a dedicated experiment is conducted. The force signal is converted into the current signal of the RY-H1's motor, which is then used to simulate haptic feedback. In the experiment, the RY-H1's index finger is brought into contact with a rigid sphere, as shown in Fig. 8. The contact force, measured by the RY-H1's DIP motor, is denoted as F_b . This force signal is then used to trigger the LRA on the user's corresponding fingertip, providing vibrotactile feedback. When the applied force exceeds 1 N (equivalent to 65 mA), the force feedback system is activated, causing the cable to tighten and generate resistive feedback F_c , as shown in Fig. 8(b).

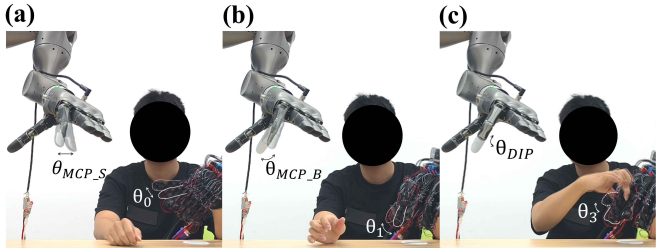


Fig. 7: Basic movements of the 3-DoF finger joints. (a) MCP joint split. (b) MCP joint bend. (c) DIP joint flexion.

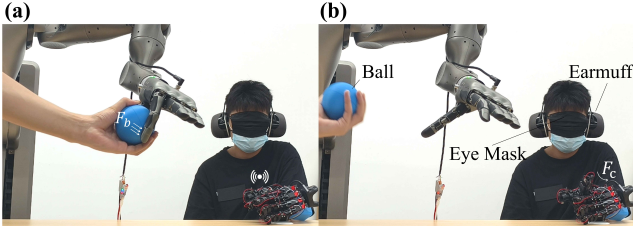


Fig. 8: Schematic diagram of the overall haptic feedback process. (a) represents the vibration signal when force is applied to the index finger. (b) represents the generation of cable-driven feedback.

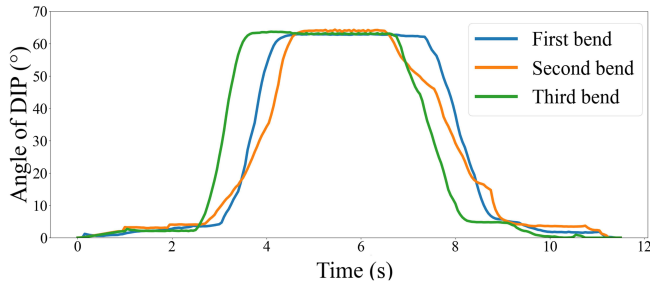


Fig. 9: Results of three repeated positioning experiments for the index finger DIP joint.

This force counteracts the user's input, effectively halting further flexion and creating a pulling sensation back towards the finger's straighter, initial posture. Fig. 10 presents detailed information on the haptic feedback process for the index finger: Fig. 10(a) shows the current variation curve of the RY-H1 during the experiment, while Fig. 10(b) displays the waveform of the LRA and the servo angle variation curve, including mode switching. Experimental results indicate that the response time for cable-driven force feedback, based on the current information from the RY-H1, is approximately 200ms.

Finally, a bottle grasping experiment based on haptic feedback is conducted, as shown in Fig. 11. Tests are performed under two conditions: with eye mask and earmuff, and without eye mask or earmuff. Each condition is further divided into trials with and without haptic feedback. The success rate of grasping a water bottle under these scenarios is summarized in Table IV, where haptic feedback is denoted as F and the use of eye mask and earmuff as E. Experimental results show that, under the eye mask and earmuff condition, the introduction of haptic feedback increases the success rate from 10% to 50%, representing a fourfold improvement. Similarly, in the absence of eye mask and earmuff, haptic feedback increases the success rate from 70% to 90%.

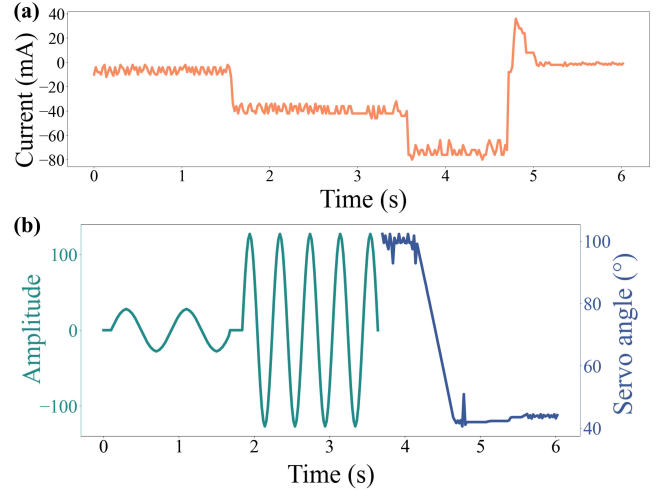


Fig. 10: Haptic feedback process information for the index finger. (a) shows the current variation curve of the RY-H1. (b) presents the waveform of the LRA and the servo angle variation curve, including mode switching.



Fig. 11: Bottle grasping experiment based on haptic feedback.

TABLE IV: Performance for Grasping a Water Bottle

Condition	Success Rate	Average Completion Time (s)
$\checkmark F \checkmark E$	5/10	8.52
$\times F \checkmark E$	1/10	18.30
$\checkmark F \times E$	9/10	2.51
$\times F \times E$	7/10	3.11

These findings validate the effectiveness and importance of the haptic feedback system in teleoperation tasks.

3) *CDF-Glove Repeated Positioning Performance*: To evaluate the fingertip repeated positioning accuracy of the CDF-Glove, we perform experiments on the index finger DIP joint. The index finger is first reset to the zero position. The finger then flexes to a specific angle (so that the fingertip touches an object), and subsequently returns to the zero position. This process repeats three times. We calculate the mean and standard deviation of the contact angle, resulting in an average value of 63.15° , with standard deviations of 0.29° , respectively. As shown in Fig. 9, the standard deviation of repeated positioning for the index finger distal joint (DIP) using the CDF-Glove is less than 0.4° , indicating high accuracy and stability.

B. CDF-Glove System Modeling Validation

To validate the effectiveness of the finger joint kinematic model proposed in Sec. IV-A, experiments were conducted

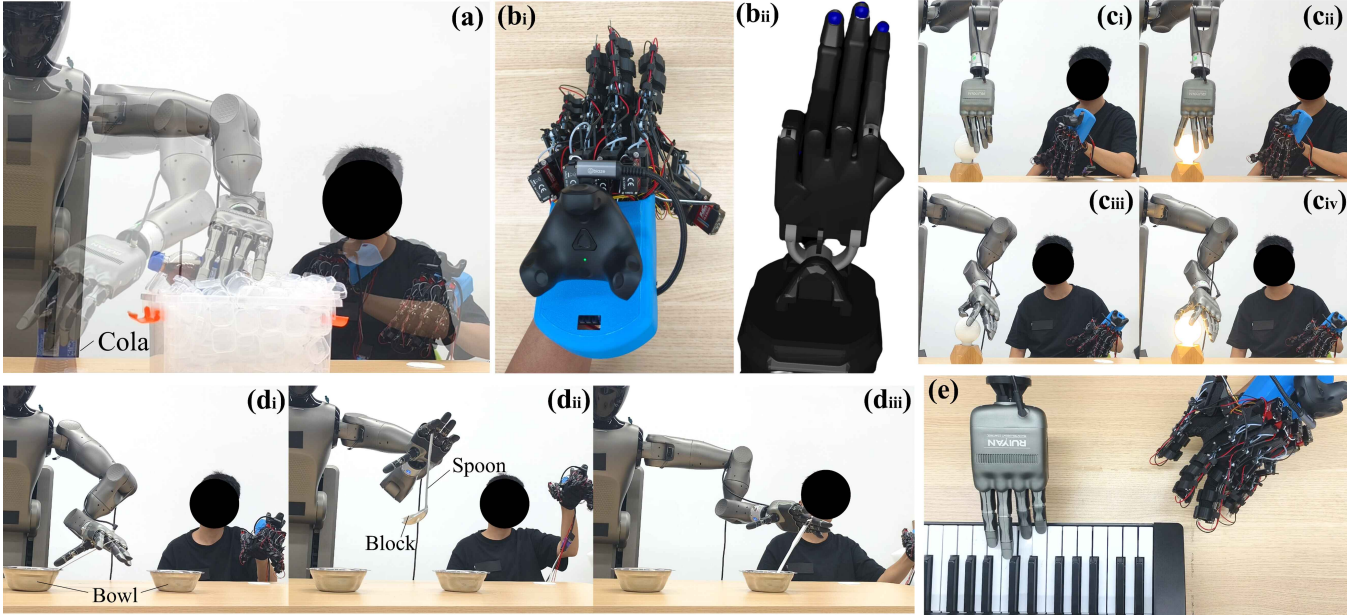


Fig. 12: Demonstrations of various tasks using the CDF-Glove. (a) Cola transportation task: removing a cola bottle from a box and placing it upright on the table. (b) Gesture demonstration: performing hand gestures based on the SDH model. (c) Manipulation task: rotating a light bulb with one or two fingers to turn it on. (d) Transport task: moving a spoon and the block on top of it from one bowl to another. (e) Manipulation task: playing the piano.

using three dexterous hands with different DoF: the 6-DoF RY-H2, the 15-DoF RY-H1, and the 24-DoF Shadow Dexterous Hand (SDH). The operation tasks for RY-H2 are verified in Sec. V-C. For RY-H1, validation is performed through grasping, transporting, and manipulation tasks, as illustrated in Fig. 12. For example, a cola bottle is grasped and placed upright on the table, requiring precise haptic feedback to control the hand posture and rotate the bottle. A spoon with a block is transported from one bowl to another, necessitating stable and accurate finger coordination throughout the process. Additional tasks such as piano playing and light bulb rotation (using single or dual fingers) further demonstrate the teleoperation capabilities of the CDF-Glove. For the SDH, validation is performed in simulation through gesture demonstrations. Each finger features four active DoF, allowing both DIP and PIP joints to be actively controlled and thus effectively verifying the correctness of (2). Experimental results show that the CDF-Glove, based on the kinematic model proposed in Sec. IV-A, enables effective motion control of varying dexterous hands.

C. Bimanual CDF-Glove Teleoperation Data Collection

To verify the high-quality data acquisition capability of the CDF-Glove, we conduct bimanual teleoperation data collection experiments (use *AGIBOT*). Bimanual tasks place significant demands on the coordination and dexterity of both hands and arms, emphasizing collaborative performance and fully demonstrating the CDF-Glove’s ability to capture data in complex scenarios. Furthermore, successful completion of these tasks supplements the experiments on the RY-H2 described in Sec. V-B. The user wears two CDF-Glove devices and utilizes two trackers to track the wrist positions and orientations, enabling teleoperation of two RY-H2 to perform

tasks such as stacking paper cups and transferring a plastic film roll, as illustrated in Fig. 13(a) and (c). For fingers other than the thumb, we map the DIP joint to the RY-H2. For the thumb, both the IP and TM(S) joints are mapped to the RY-H2. Throughout the experiments, the user flexibly adjusts finger postures and applies tactile sensation according to the specific requirements of each task. The entire data acquisition pipeline operates at approximately 30 Hz. Collected data include fourteen joint angles for both arms, one vertical displacement measurement, six joint angles for each RY-H2, and image information. The image data are acquired using a *Realsense D455* camera and two *Realsense D405* cameras.

D. Diffusion Policy on Collected Data

To evaluate the quality of the data collected using the CDF-Glove, we employ the IL method known as Diffusion Policy [6], which has demonstrated impressive performance in various robotic manipulation tasks. For each task, we train the Diffusion Policy models on two datasets: one collected using the CDF-Glove (see Sec. V-C) and the other collected via kinematic teaching (KT). Both datasets consist of 200 teleoperated demonstrations for the cup stacking task and another 200 for the plastic film roll transfer task, totaling 400 demonstrations per dataset. The training procedure for both models is identical, with each trained for 1000 epochs.

The validation results of the Diffusion Policy models for both tasks and datasets are presented in Table. V. The execution of the trained models on the two tasks is illustrated in Fig. 13(b) and (d). It can be observed that the dataset collected with CDF-Glove is of higher quality than the KT dataset: it raises average success by 55%, shortens completion time by 15.19 seconds (a 47.2% relative reduction).

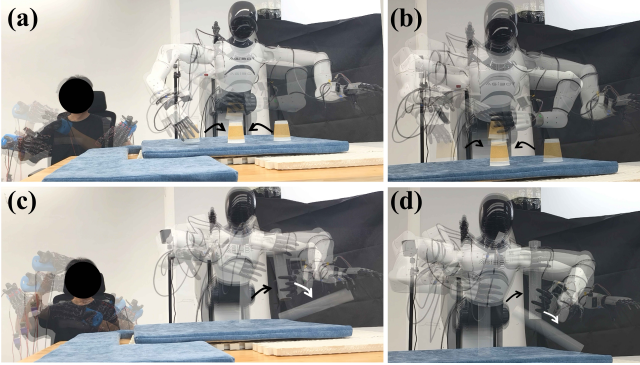


Fig. 13: Bimanual data collection. (a) Teleoperate cup stacking. (b) Cup stacking using the trained model. (c) Teleoperate plastic film roll transfer. (d) Plastic film roll transfer using the trained model.

TABLE V: Success Rate and Completion Time for the Two Tasks

Condition	Success Rate	Average Completion Time (s)
CDF (Cup Stacking)	10/10	14.74
KT (Cup Stacking)	4/10	28.91
CDF (Film Roll Transfer)	8/10	19.49
KT (Film Roll Transfer)	3/10	35.70

VI. CONCLUSION AND FUTURE WORK

This work presents the CDF-Glove: a lightweight, high-degree-of-freedom, cable-driven force-feedback glove fabricated for \$230.51. The device attains 0.4° repeatability in distal-joint positioning and delivers force feedback within 200 ms. Comprehensive kinematic models of finger-joint angles and cable-tracking are derived and experimentally verified. Compared with KT, bimanual data acquisition with the CDF-Glove followed by IL increases task success by 55% and reduces mean completion time by 15.19 seconds (a 47.2% relative reduction). Current limitations include restricted force output, lack of complex haptic feedback, encoder signal drift and zero-offset fluctuation, as well as PCB-induced control latency. Ongoing work will intensify force output, refine the PCB to minimize latency, and expand applications to virtual reality and telesurgery.

REFERENCES

- [1] B. D. Argall, S. Chernova, M. Veloso, and B. Browning, “A survey of robot learning from demonstration,” *Robotics and Autonomous Systems*, vol. 57, no. 5, pp. 469–483, 2009.
- [2] H. Liu, X. Xie, M. Millar, M. Edmonds, F. Gao, Y. Zhu, V. J. Santos, B. Rothrock, and S.-C. Zhu, “A glove-based system for studying hand-object manipulation via joint pose and force sensing,” in *2017 IEEE/RSJ International Conference on Intelligent Robots and Systems (IROS)*, 2017, pp. 6617–6624.
- [3] H. Liu, Z. Zhang, X. Xie, Y. Zhu, Y. Liu, Y. Wang, and S.-C. Zhu, “High-fidelity grasping in virtual reality using a glove-based system,” in *2019 International Conference on Robotics and Automation (ICRA)*, 2019, pp. 5180–5186.
- [4] H. Zhang, S. Hu, Z. Yuan, and H. Xu, “Doglove: Dexterous manipulation with a low-cost open-source haptic force feedback glove,” *arXiv preprint arXiv:2502.07730*, 2025.
- [5] I. Sarakoglou, A. Brygo, D. Mazzanti, N. G. Hernandez, D. G. Caldwell, and N. G. Tsagarakis, “Hexotrac: A highly under-actuated hand exoskeleton for finger tracking and force feedback,” in *2016 IEEE/RSJ International Conference on Intelligent Robots and Systems (IROS)*, 2016, pp. 1033–1040.
- [6] C. Chi, Z. Xu, S. Feng, E. Cousineau, Y. Du, B. Burchfiel, R. Tedrake, and S. Song, “Diffusion policy: Visuomotor policy learning via action diffusion,” *The International Journal of Robotics Research*, 2024.
- [7] T. He, Z. Luo, W. Xiao, C. Zhang, K. Kitani, C. Liu, and G. Shi, “Learning human-to-humanoid real-time whole-body teleoperation,” in *2024 IEEE/RSJ International Conference on Intelligent Robots and Systems (IROS)*. IEEE, 2024, pp. 8944–8951.
- [8] Y. Qin, W. Yang, B. Huang, K. Van Wyk, H. Su, X. Wang, Y.-W. Chao, and D. Fox, “Anyteleop: A general vision-based dexterous robot arm-hand teleoperation system,” in *Robotics: Science and Systems*, 2023.
- [9] X. Cheng, J. Li, S. Yang, G. Yang, and X. Wang, “Open-television: Teleoperation with immersive active visual feedback,” in *Conference on Robot Learning*. PMLR, 2025, pp. 2729–2749.
- [10] S. P. Arunachalam, I. Güney, S. Chintala, and L. Pinto, “Holo-dex: Teaching dexterity with immersive mixed reality,” in *2023 IEEE International Conference on Robotics and Automation (ICRA)*, 2023, pp. 5962–5969.
- [11] C. Wang, H. Shi, W. Wang, R. Zhang, L. Fei-Fei, and K. Liu, “Dexcap: Scalable and portable mocap data collection system for dexterous manipulation,” in *RSS 2024 Workshop: Data Generation for Robotics*, 2024.
- [12] K. Shaw, Y. Li, J. Yang, M. K. Srirama, R. Liu, H. Xiong, R. Mendonca, and D. Pathak, “Bimanual dexterity for complex tasks,” in *Conference on Robot Learning*. PMLR, 2025, pp. 5166–5183.
- [13] P. Naughton, J. Cui, K. Patel, and S. Iba, “RespiLOT: Teleoperated finger gaitting via gaussian process residual learning,” in *Conference on Robot Learning*. PMLR, 2025, pp. 4410–4424.
- [14] Q. Ben, F. Jia, J. Zeng, J. Dong, D. Lin, and J. Pang, “Homie: Humanoid loco-manipulation with isomorphic exoskeleton cockpit,” in *RSS 2025 Workshop on Whole-body Control and Bimanual Manipulation: Applications in Humanoids and Beyond*, 2025.
- [15] T. Zhao, V. Kumar, S. Levine, and C. Finn, “Learning fine-grained bimanual manipulation with low-cost hardware,” *Robotics: Science and Systems XIX*, 2023.
- [16] H. Fang, C. Wang, Y. Wang, J. Chen, S. Xia, J. Lv, Z. He, X. Yi, Y. Guo, X. Zhan *et al.*, “Airexo-2: Scaling up generalizable robotic imitation learning with low-cost exoskeletons,” in *7th Robot Learning Workshop: Towards Robots with Human-Level Abilities*, 2025.
- [17] S. Furuya, T. Oku, H. Nishioka, and M. Hirano, “Surmounting the ceiling effect of motor expertise by novel sensory experience with a hand exoskeleton,” *Science Robotics*, vol. 10, no. 98, p. eadn3802, 2025.
- [18] N. Popescu, D. Popescu, M. Ivanescu, D. Popescu, C. Vladu, C. Berceanu, and M. Poboroniuc, “Exoskeleton design of an intelligent haptic robotic glove,” in *2013 19th International Conference on Control Systems and Computer Science*, 2013, pp. 196–202.
- [19] W. Xu, Y. Liu, and P. Ben-Tzvi, “Development of a novel low-profile robotic exoskeleton glove for patients with brachial plexus injuries,” in *2022 IEEE/RSJ International Conference on Intelligent Robots and Systems (IROS)*, 2022, pp. 11121–11126.
- [20] R. Chauhan, B. Sebastian, and P. Ben-Tzvi, “Grasp prediction toward naturalistic exoskeleton glove control,” *IEEE Transactions on Human-Machine Systems*, vol. 50, no. 1, pp. 22–31, 2020.
- [21] D. Wang, Y. Wang, J. Pang, Z. Wang, and B. Zi, “Development and control of an mr brake-based passive force feedback data glove,” *IEEE Access*, vol. 7, pp. 172477–172488, 2019.
- [22] N. Takahashi, S. Furuya, and H. Koike, “Soft exoskeleton glove with human anatomical architecture: Production of dexterous finger movements and skillful piano performance,” *IEEE Transactions on Haptics*, vol. 13, no. 4, pp. 679–690, 2020.
- [23] I. Cerulo, F. Ficuciello, V. Lippiello, and B. Siciliano, “Teleoperation of the schunk s5fh under-actuated anthropomorphic hand using human hand motion tracking,” *Robotics and Autonomous Systems*, vol. 89, pp. 75–84, 2017.
- [24] L. L. Radulovic and Z. W. Wojcinski, “Ptfe (polytetrafluoroethylene; teflon®),” in *Encyclopedia of Toxicology (Fourth Edition)*, fourth edition ed., P. Wexler, Ed. Oxford: Academic Press, 2024, pp. 1001–1006.
- [25] Y. Park, J. Lee, and J. Bae, “Development of a wearable sensing glove for measuring the motion of fingers using linear potentiometers and flexible wires,” *IEEE Transactions on Industrial Informatics*, vol. 11, no. 1, pp. 198–206, 2015.
- [26] Y. Dong, X. Liu, J. Wan, and Z. Deng, “Gex: Democratizing dexterity with fully-actuated dexterous hand and exoskeleton glove,” 2025.